# Bubble-raft collapse and the nonequilibrium dynamics of two-state elastica

Chin-Chang Kuo, Devin Kachan, Alex J. Levine, and Michael Dennin

# Bubble raft collapse and the nonequilibrium dynamics of two-state elastica

Chin-Chang Kuo[1*] and Devin Kachan[3], Alex J. Levine[3,4,5], and Michael Dennin[1,2]

[1]*Department of Physics and Astronomy, University of California, Irvine*
[2]*Institute for Complex Adaptive Matter, University of California, Irvine*
[3]*Department of Physics & Astronomy, University of California, Los Angeles*
[4]*Department of Chemistry & Biochemistry, University of California, Los Angeles and*
[5]*Department of Biomathematics, University of California, Los Angeles*

We report on the collapse of bubble rafts under compression in a closed rectangular geometry. A bubble raft is a single layer of bubbles at the air-water interface. A collapse event occurs when bubbles submerge beneath the neighboring bubbles under compression, causing the structure of the bubble raft to go from single-layer to multi-layer. We studied the collapse dynamics as a function of compression velocity. At higher compression velocity we observe a more uniform distribution of collapse events, whereas at lower compression velocities the collapse events accumulate at the system boundaries. We propose that this system can be understood in terms of a linear elastic sheet coupled to a local internal (Ising) degree of freedom. The two internal states, which represent one bubble layer versus two, couple to the elasticity of the sheet by locally changing the reference state of the material. By exploring the collapse dynamics of the bubble raft, one may address the basic nonlinear mechanics of a number of complex systems in which elastic stress is coupled to local internal variables.

PACS numbers:

## I. INTRODUCTION

There are a number of soft matter systems exhibiting highly nonlinear elasticity, at least in part due to the complex interplay of elasticity and internal state variables. Some examples include colloidal crystals and worm-like micellar solutions, which exhibit banding [1, 2] under applied shear stress, monolayers and membranes that form localized folds [3] under compression, and biopolymers such as DNA [4–8] or alpha-helical polypeptides [9, 10] that can kink (and locally melt) under torque. There are significantly more complex many-body systems that generate nonlinear responses to applied stress via the adaptation of the internal dynamics of the constituent elements in response to applied stress. In many cases these internal dynamics are poorly understood, but for the purposes of elucidating their collective mechanical response, these internal states may be reduced to one of a small number of states. For example, in studies of tissue dynamics, the rate of cell division in tissues appears to depend on applied stress [11, 12], and this mechanical nonlinearity has been suggested to play a key role in the pattern formation [13] in tissues, the development of flowers [14], and the invasion of tumors into surrounding healthy tissue [12, 15].

A minimal description of these complex systems can be formed in terms of an elastic manifold coupled to a discrete internal variable that determines elastic properties in at least one of two distinct ways. In the first case, the state of elastic stress causes local transitions in the material's elastic constants; for example, in shear banding and biopolymer kinking, the material's elastic constants locally transition from a stiff state to a less stiff one. To be more precise in the case of polypeptides, bending can disrupt local hydrogen bonding in the helix, and in DNA may induce local melting, which corresponds to the breakdown of the base-pairing interaction. These changes in internal molecular configurations affect the local bending modulus of the biopolymer. For example, local DNA melting decreases the bending modulus by a factor of about fifty. Because the transition is to a softer state of the elastic body at the expense of increasing the local free energy of the chain, the system trades elastic strain energy for locally increasing its internal free energy. This leads to a nonlinear strain softening of the elastic body driven by the creation of localized "defects" of the softer, but thermodynamically disfavored internal configuration. Such effects have been explored using a simple model – the helix-coil worm-like chain [9, 10]; we refer to this nonlinear coupling between elasticity and internal state variables as a type I coupling.

In contrast, the underlying elastic reference state, i.e., the state of zero strain, can itself evolve by e.g., cell division in a tissue. When that local rate of cell division itself depends on the state of stress, even a tissue in the linear elastic regime can exhibit complex, nonlinear responses to applied stress. There is also an inorganic example to be found in $CeO_2$ thin films with nanoscale pores, developed for use as supercapacitors [16]. In such materials, charge storage occurs through the absorption of Li ions, which lead to a local expansion of the pores, changing the elastic reference state of the material. We refer to these systems as having a type II coupling, and they will be the focus of the current studies using bubble rafts.

There is a long history in condensed matter physics of using bubble rafts as models of atomic solids. By taking advantage of the $\sim 10^7$ increase in scale between

*email:chinchak@uci.edu

bubbles and atoms, one may more easily visualize features such as the motion of topological defects in crystals [17, 18], stress relaxation [19] and shear-banding in disordered materials [21–23]. In this article we propose that bubble rafts may also be used to explore the interplay of elasticity and local internal variables that control the elastic reference state. This class of problems is of particular interest with regard to modern studies of tissue growth and morphology. We perform experiments on the compression of a disordered elastic solid composed of a monolayer of bubbles at the air/water interface. The total number of bubbles is essentially fixed over the time of a typical experiment. But, under sufficient compression, this system stochastically forms local regions of double bubble layers, the second layer being submerged under the one at the surface. The doubling of the layer can be treated as an elementary example of a discrete (two-state or Ising) variable coupled to stress in the effectively two-dimensional elastic manifold of the interfacial bubble layer. Because the submerged bubble layer does not form a continuous, stress-bearing network, the local transition between the single and double layer can be represented as a local discrete change in the elastic reference state – the material jumps between a lower density (single layer) and higher density (double layer) state. Thus the bubble layer is a simple model of a two-dimensional elastic manifold with type II interactions, using the terminology introduced above.

In this case, the simple advantage of scale is less pronounced because the bubbles are typically only one hundred times larger than cells, but there are other advantages stemming from the simplicity of the bubble raft. By eliminating the biological complexity of the tissue, such as chemical signaling and the active generation of internal stresses, the bubble raft system allows one to develop and test fundamental models of type II nonlinear elasticity. The bubble raft also provides experimental advantages in terms of time scale. The collapse dynamics we study occurs on time scales of one to one thousand seconds, and is thus slow enough to be amenable to video tracking but fast enough to run multiple experiments rapidly. We believe there are direct applications of these results to more complex systems including tissue growth and membrane or monolayer folding.

We report on experiments exploring the collapse dynamics in a disordered bubble raft in a closed rectangular geometry, focusing specifically on determining the spatial probability distribution for double layer formation as a function of compression speed. The rate-dependence of the single- to double-layer transition demonstrates the fundamentally nonequilibrium nature of the dynamics. From a simple analysis of the compression modulus of the bubble raft and its viscous flow over the aqueous subphase, it is clear that the elastic compression mechanically equilibrates rapidly on experimental time scales. The single layer/double layer variable, however, is slow. It falls out of equilibrium, trapping the system temporarily in higher energy metastable states, which then slowly

relax through the formation of double layer domains.

We also propose a general model to describe the elasticity of any linear elastic solid in which the strain-free state of the material can discontinuously switch between two states – a type II elastic nonlinearity. We explore an elementary, one-dimensional example of this model to study the nonequilibrium dynamics of double layer domain growth in the compressed system, using Glauber spin dynamics to account for the single-to-double layer transitions. The predictions of the model for the spatial probability distribution of such transitions as a function of compression speed are then compared to experiments

The remainder of the article is organized as follows. In section II we detail the bubble raft collapse experiments, and demonstrate the stochastic double-layer formation kinetics under compression in section III. In section IV, we develop the minimal model of this type II nonlinear elasticity using an Ising variable representing the single layer/double layer degree of freedom, coupled to the linearly elastic bubble layer. We then explore a one-dimensional example of this model. In our discussion, we compare the model predictions to our experiments, discuss open questions, and propose future work.

## II. EXPERIMENTAL DETAILS

The bubble raft was prepared by flowing compressed nitrogen through a needle under the bubble solution. The bubble solution contains 15% of glycerol, 5% Miracle Bubble, and 20% deionized water. The focus of this study is the amorphous system composed of bubbles with radii in the range of 0.3 mm to 0.5 mm. These polydisperse bubble rafts were created by oscillating the needle during bubble formation, generating small variations in bubble size. The initial state is a contiguous array of bubbles that fill the trough surface, forming a continuous elastic sheet. Before compression, the typical gas-area packing fraction for our bubble raft (i.e., the fraction of the bubble raft area taken up by the bubbles) is $\approx 0.86$. Details of the bubble raft preparation can be found in our previous work [28].

The experimental setup is shown in Fig. 1. The initial bubble raft size is described as $L \times W_0$ for its initial length and width, respectively. We considered two different initial geometries for the bubble raft: 8cm × 6cm and 8cm × 10cm. This allowed for an initial test of system size and/or aspect ratio effects. No obvious impact of systems size or aspect ratio was observed, and the results presented here all are from the 8 cm × 10 cm system.

The focus of the study was on the impact of the compression velocity on the probability of double layer formation. Compression of the bubble raft was achieved through two movable barriers that were controlled by a single stepper motor. The bubble rafts were compressed at a constant velocity, which ranged from $1 \times 10^{-4}$ mm/s to $1 \times 10^2$ mm/s. The compressive strain in our experiment is defined as $\frac{L_0 - L}{L_0} = \Delta L / L$, where $L_0$ is the initial
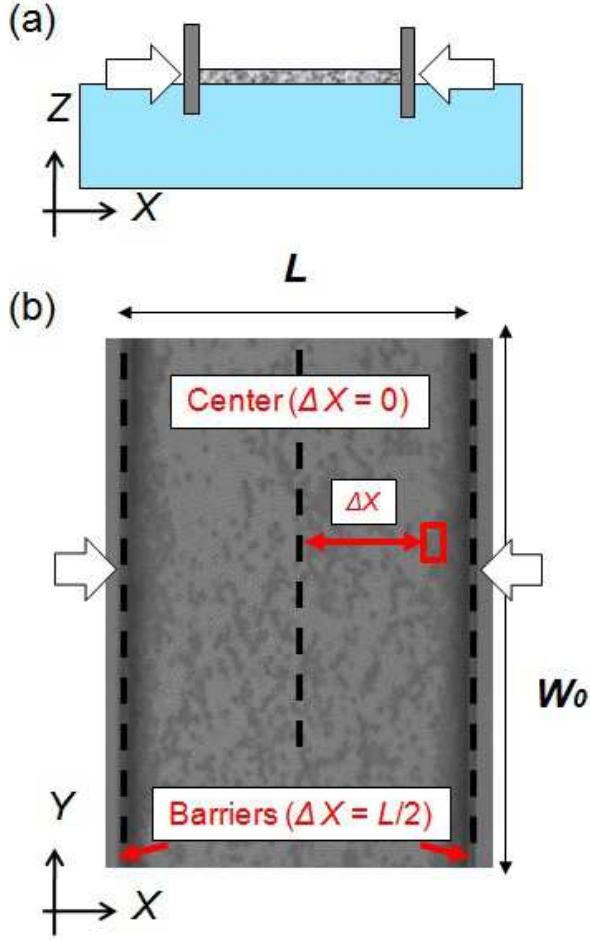
FIG. 1: (color online) (a) A schematic of the experimental setup and the geometry for the bubble raft. We applied the compressive strain by moving the barriers towards to the center. (b) A typical image of the compressed bubble raft. Darker areas show doubling of the bubble monolayer and $\Delta X$ indicates distances measured from the center line of the system.



FIG. 2: Typical images of amorphous bubble raft under compression at the same amount of the compressive strain ($\sim 0.66$) with different compression velocities. (a)(b)are images with the compression velocity of 0.0086 mm/s and 8.6 mm/s. The initial size is 8 cm $\times$ 10 cm and the average bubble radius is 0.4 mm for both sets of experiment. The scale bars in images are 2 cm. A comparison of these images illustrates the increased nucleation rate of double layers in the middle of the raft when it is compressed at higher rates.

raft length.

Bubble raft collapse images were recorded by a CCD camera with a maximum frame rate of 30 s$^{-1}$. Over the observable timescales, the stepper motor reaches its steady-state velocity essentially instantaneously. The bubbles also reach their terminal velocity very rapidly on these timescales. One can make a simple estimate of this time from the ratio of the Stokes drag on the bubble to its mass. We estimate the bubble's mass to be $4\pi a^2 t\rho$ (where t is the thickness of the bubble, $\approx 10^{-4}$cm and $\rho$ is the density of water), to arrive at a bubble mass of $\sim 10^{-6}$g. We also estimate the Stokes drag on a bubble of radius $a$ and velocity $v$ to be $\approx \eta a v$, where $\eta$ is the dynamical viscosity of water. Thus, we find the time for the bubble to accelerate to its terminal velocity is on the order of $10^{-3}$ s, which is not observable at our current frame rates. Consequently, we do not observe the acceleration of bubbles or any dynamical transients asso-
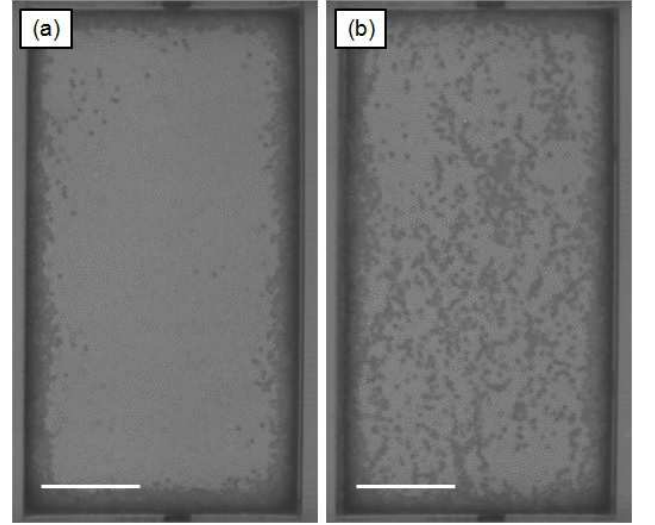
ciated with the acceleration of the barriers. In addition, bubble coarsening does not occur over the time scales of two hours in our experiment, consistent with previous studies [29].

We used MATLAB to perform image processing and analysis. With appropriate lighting and thresh-holding of images, the single and double layers were distinguished by their difference in overall brightness. These intensity variations were used to identify collapse events.

## III. EXPERIMENTAL RESULTS

Figure 2 illustrates the qualitative difference between the collapse dynamics of amorphous bubble rafts at slow (a, left) and fast (b, right) compression velocities. The compression velocity of Fig. 2(a)(b) are 0.0086 and 8.6 mm/s, respectively. Both cases had the same initial size of 8 cm $\times$ 10 cm. To compare the collapse distribution at different compression velocities, we consider of equal the raft at equal values of compressive strain ($\Delta L/L_0$). The images in Fig. 2(a) and (b) were both made at a compressive strain of $\sim 0.66$. For the system with the higher compression velocity, the collapse events are uniformly distributed throughout the raft; whereas for the slower speed, nucleation of multiple layers near the boundary dominate the dynamics. Also, the overall density of collapse events appears to be greater for the faster speeds.

We also examined monodisperse bubble rafts with poly-crystalline structure. Here we focus on the amor-

phous bubble rafts as this provides a simpler elastic system. The more ordered, monodisperse bubble rafts, exhibited double layer growth that propagated along particular crystallographic axes. We will consider this behavior in detail in future work.

To study the effect of compression velocity on the nucleation dynamics, we focus on the formation of double layers. As discussed above, double layers are identified using the different intensity levels for the single- versus double-layer regions. Using this analysis, we also observe multilayer regions (greater than two) near the boundaries. The penetration length of higher order multi-layers ranged from $\approx 3$ mm to 1 cm over the course of compression. We avoid taking data on this boundary regime by focussing on the central region of the trough, where only single and double layers are observed.

The formation of the double layer regions is a stochastic event so that the precise trajectory of double-layer formation is irreproducible. Given the macroscopic energies involved in the transition from single to double layer, the underlying source of stochasticity is nonthermal. Multiple experiments, however, allow one to build up the probability density of collapse events (i.e., the transition from a single to a double layer) as a function of both space and time. We compute the probability of a collapse event occurring a fixed distance away from the compression barrier using the following procedure (that is shown schematically in Fig. 1). We assume that the probability of a collapse event is homogeneous along the direction parallel to the barriers. Thus, we may average the fraction of single layer in vertical slices taken parallel to the barriers to obtain this probability. The position of the vertical slices is defined relative to the center of the trough - so that the zero position is fixed and positions left of center are negative. It will prove convenient when discussing the comparison between these experiments and our theory to convert the measured double-layer probability $P_i$ into "spin" variable via $s_i = 2P_i - 1$. Thus, $-1 < s < +1$ corresponding to double layer probabilities running from 0 to 1. In order to compare the dynamics at different compression rates, we used the compressive strain $\Delta L/L_0$ as our measure of "time." Finally, due to the decrease in system length, we normalized the off-center distance by half of the compressed raft length $(2\Delta x/L)$.

Typical probability distributions for the formation of a multilayer are shown for low (0.0086 mm/s), medium ( 0.43 mm/s) and high (8.6 mm/s) compression velocities in Figs. 3 (a), (b), and (c). The color code, which runs from $s = -1$ (red) to $s = 1$ (yellow), shows the statistical result for single layer and double layer. In general, a high probability of collapse events accumulates at the boundary and propagates inward for both fast and slow compression velocities. The growth dynamics of collapsed raft probability near the center of the trough, however, are quite distinct for slow and rapid compression. For slow compression velocity, collapse probability continuously and gradually propagates inward from the
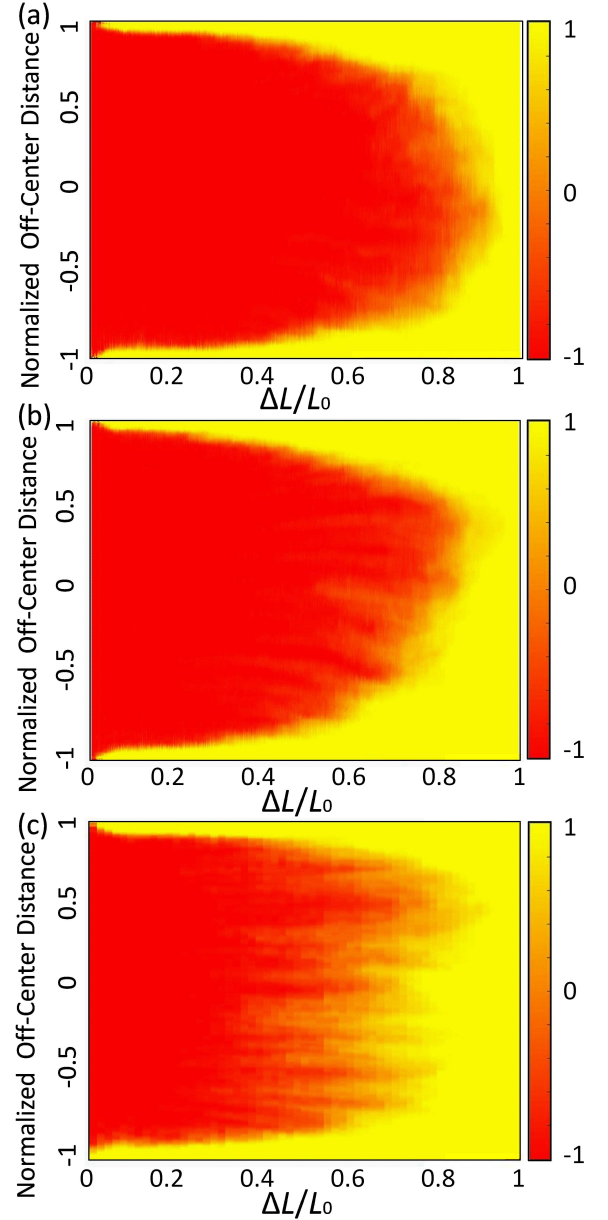


FIG. 3: The probability of double layer formation expressed in terms of $-1 < s < 1$ (red to yellow) as a function of normalized off-center distance at a fixed total compressive strain of 0.85. (a), (b), and (c) show results for compression velocities of 0.0086, 0.43, and 8.6 mm/s respectively.

boundaries towards the center, as shown in Fig. 3(a). In contrast, at fast compression velocity, the collapse probability initially propagates continuously inward from the boundaries, but at a critical strain of $\approx 0.25$, the collapse probability rapidly jumps in the central part of the bubble raft. Upon reaching the compressive strain of 0.55, the whole surface of the bubble raft is a double (multi-) layer structure. Thus, the stochastic dynamics of double layer formation depends strongly on the compression

velocity.

## IV. THEORY

### A. Multilayer raft elasticity

To explore the collapse dynamics theoretically, we consider a simple, one-dimensional model of the bubble layer [30]. We treat the two-dimensional bubble layer as elastically equivalent to a one-dimensional array of Hookean springs with spring constant $k$. To account for the change in elastic reference state upon local layer collapse, each spring selects one of two possible rest lengths; the longer one corresponds to the single layer configuration and the shorter to the double layer configuration. Thus, when compressed, elastic energy in the spring chain can be reduced by transitions of some (or all) springs from the longer to the shorter rest length.

We write the elastic energy of the spring chain

$$H_{\text{el}} = \frac{k}{2} \sum_{i=0}^{N-1} \left[ u_{i+1} - u_i + \Delta(\sigma_i) \right]^2 \qquad (1)$$

in terms of the displacements of the spring ends (nondimensionalized by the bubble radius $a$) $u_i$. The rest lengths of the springs depend on a discrete, Ising-type variable $\sigma$, which takes the values $-1$ and $+1$ when the bubble layer is in its expanded single layer or compressed double-layer configuration, respectively. In other words, we require that

$$\Delta(\sigma) = \begin{cases} \Delta_> & \sigma = +1 \\ \Delta_< & \sigma = -1 \end{cases}, \qquad (2)$$

where, as implied by the notation: $\Delta_> > \Delta_<$. Since the length $\Delta_>$ corresponds to two bubble radii $2a$, and the shorter separation corresponds to only one, we expect that $\Delta_> - \Delta_< = a$, although one is not required to make this assumption in the more general implementation of the model. We neglect the possibility of triple and higher order layerings of the bubble raft. While these appear near the walls in the experiment, they are not observed in the interior of the bubble layer.

To complete the description of the energetics of a layer configuration, we include a simple Ising description of the layer variables $\sigma_i$:

$$H_s = -J \sum_{i=0}^{N-1} \sigma_{i+1} \sigma_i + h \sum_{i=0}^{N-1} \sigma_i. \qquad (3)$$

The implications of this description are two-fold. We assume a "ferromagnetic" coupling $J > 0$ for the layer variables, which implies that there is domain wall energy associated with the transition between single and double layers. This results from the fact that bubbles on the boundary of the double layer necessarily have fewer contacting bubbles and thus suffer a larger surface energy cost due to their position. The second term, representing an applied magnetic field in the standard Ising description allows for a fixed energy cost per area associated with the formation of a double layer; for each transition: $\sigma_i : -1 \to +1$, the energy of the configuration increases by $2h$. We attribute this term to the (very small) effects of buoyancy, although the energetic effects of different packings in the first and second bubble layers cannot be entirely discounted as contributing to this term as well. Finally, we expect that $h \ll J$ for the bubble raft, as explained in section IV C.

The combination of Eqs. 1, 3 completes our description of the energetics of the model. Of course, any predictions made regarding the stochastic dynamics of double layer creation relies not only on the energetics of the system, but also on the assumptions regarding the source of noise in this inherently nonequilibrium system. There are multiple nonthermal noise sources present including vibrations coming from the motor used to change the area of the bubble raft and other ambient sources of vibration in the lab. The simplest assumption one can make is to treat this as Gaussian white noise acting on all of the degrees of freedom in an uncorrelated manner. This is equivalent to assuming an effective noise temperature. In what follows we make this assumption, but suppress all references to temperature to avoid any confusion with the thermodynamic temperature of the system. Thus, the $J$ coupling and the symmetry-breaking field in $h$ in Eq. 3 are inherently dimensionless quantities.

### B. Raft collapse dynamics

To develop a dynamical theory for the system from the above Hamiltonian, we write overdamped (model A [26]) dynamics for the displacement field

$$\dot{u}_i = -\Gamma \frac{\partial H_{\text{el}}}{\partial u_i}, \qquad (4)$$

based on the assumption that any long range hydrodynamic interaction is sufficiently screened by the small depth of the aqueous subphase [27]. We necessarily introduce one new parameter, $\Gamma$ with dimensions of a mobility. Using Eq. 1 and Eq. 4 we write a set of differential equations for the displacement variables as

$$\dot{u}_i = k\Gamma \left[ u_{i+1} - 2u_i + u_{i-1} + \Delta \left( \sigma_i - \sigma_{i-1} \right) \right]. \qquad (5)$$

The right hand side of the above equation represents the overdamped (i.e., diffusive) relaxation of density modes in the bubble layer controlled by the constant $k\Gamma$, with dimensions of frequency. We justify the use of overdamped dynamics by appealing to the small mass and large drag forces on the bubbles; please see the discussion in Section II.

The second term on the same side of the above equation couples spin variables to the elastic stresses in the

bubble layer. To obtain this second term, we have written the relation between the elastic reference state the local spin variable as

$$\Delta(\sigma) = \frac{(\Delta_> + \Delta_<)}{2} + \Delta\sigma, \qquad (6)$$

where the constant $\Delta = (\Delta_> - \Delta_<)/2$ measures the change in the reference state associated with a local transition between the single and the double layer. The distinction between Eq. 6 and the original Eq. 2 is immaterial as long as $\sigma$ takes discrete values of $\pm 1$. We will, however, continue to use the linear form of the $\Delta(\sigma)$ when we replace the discrete spin variable $\sigma$ with a continuous one $s_i = \langle \sigma_i \rangle$ representing the ensemble average of that spin variable. We also introduce a simple Glauber-based first order differential equation to describe the dynamics of the time-dependent average of the spin-like layer number variable $s_i = \langle \sigma_i \rangle$:

$$\tau_s \dot{s}_i = -s_i + \frac{\gamma}{2}\left(s_{i+1} + s_{i-1}\right) - \tanh\left(h_{\text{eff}}(t)\right)\left[1 - \gamma\eta\right]. \qquad (7)$$

This corresponds to selecting a particular nonequilibrium dynamics for the Ising system based on single stochastic spin flips that do not conserve the total "magnetization," i.e., the amount of the system in single- or in the double-layer configuration. This sort of spin dynamics is well-described in the literature – see Ref. [24, 25]. It represents a truncation of a system of differential equations representing the dynamics of the $n^{\text{th}}$ moment of the spin distribution $\langle \sigma_1 \ldots \sigma_n \rangle$ in terms of higher moments. The Glauber dynamics enforces a closure relation at the second moment and is applicable in the limit of small applied field $h$. Fortunately, this limit is appropriate for the bubble raft system in which the energy difference per bubble between the single and double layers is small. In what follows, we will see that this approximation may break down under large compressive loading, where the elastic strain energy generates a large effective ordering field, which dominates over the inherent one $h$. We return to this point in the discussion of the results.

In the Glauber approximation, the effect of the local $J$ coupling that energetically penalizes transitions in the layer number enters the dynamical equations in terms of $\gamma = \tanh(2J)$ and $\eta = \tanh(J)$; $\gamma = 2\eta/(1+\eta^2)$. Finally, the function

$$h_{\text{eff}}(t) = \tanh\left\{h + k\Delta\left[u_{i+1}(t) - u_i(t)\right]\right\}, \qquad (8)$$

provides the effective "local magnetic field" to which the spin variables respond. The first term accounts for the (small) energy difference between the single and double layer bubble configurations that favors the single-layer geometry. The second term is the elastic correction that, under compression, is negative and that drives the local spin variable from the single-layer (-) to the double-layer (+) structure. In the standard derivation of Glauber dynamics and in our modified one as well, both $h$ and $k\Delta a$
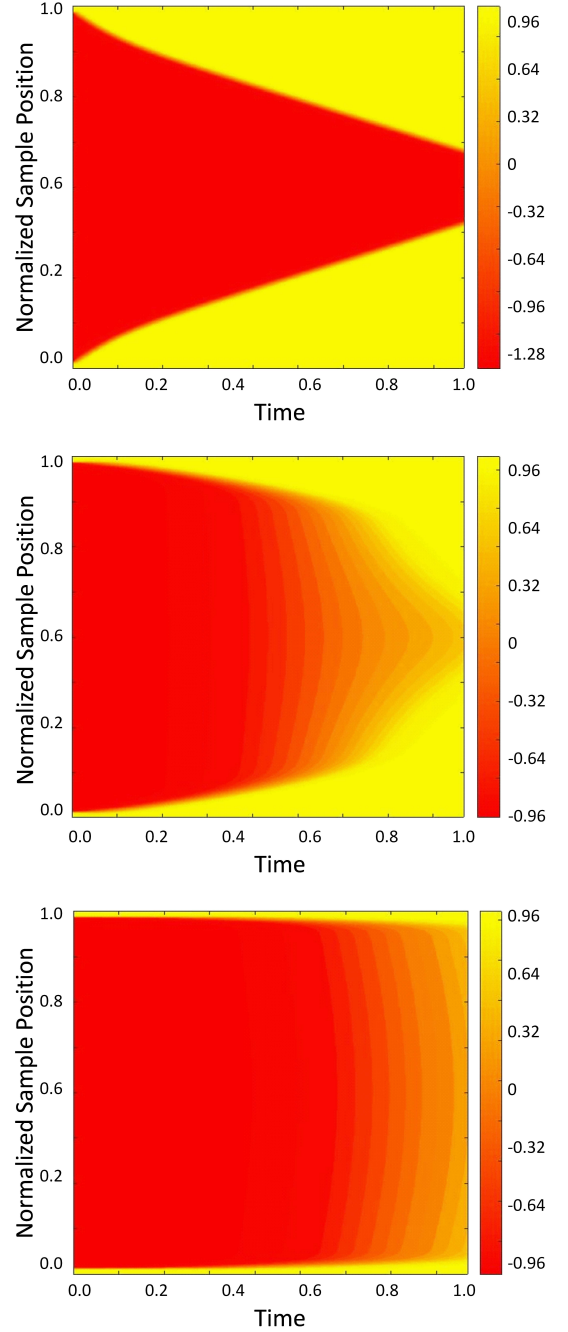


FIG. 4: (color online) Time evolution of the probability of double layer appearance measured in terms of $\langle s \rangle$ (where $s = -1$ (red), $+1$ (yellow) corresponds to single and double layers respectively) as a function of the distance from the walls. For slow compression $\bar{V} = 0.1$ (top) the double layer, stabilized by the interaction with the walls smoothly progresses inward a constant rate. At intermediate compression rates $\bar{V} = 1$ (middle), however, the probability of double-layer appearance acquires a distinct step, indicating the introduction of a quenched-in domain wall in the layer variable. At higher compression rates $\bar{V} = 10$ the number of these steps grows until they merge (bottom) and the double layer grows uniformly. In all cases velocities are given in dimensionless units – see Eq. 14 – , and $D = 10^4$, $h = 0.1$, $J = 1.0$, $\bar{\Delta} = 0.5$, and $k = 10$. The time axis has been rescaled such that the raft has the same compression at each time point in all figures ( Time $= 1$, $\Delta L/L_0 = 0.8$ ). As time progresses (to the right) lengths (vertical axis) are rescaled so that the remaining width of the raft is fixed to be unity.
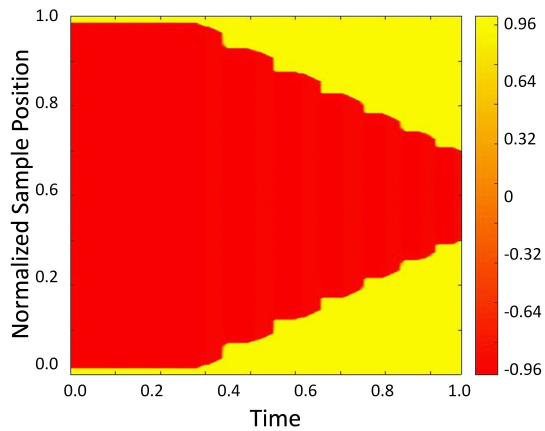
FIG. 5: (color online) Time evolution of the probability of double layer appearance as a function of the distance from the walls along the compression direction for a significantly stiffer layer: $D = 10^4$, $h = 10^{-2}$, $\bar{\Delta} = 0.5$, and $k = 10^4$ for $\bar{V} = 0.1$. For these parameters the system exhibits six distinct steps during the compression. As the velocity is increased, fewer but larger steps occur; eventually, the step size reaches the system size so a single, uniform jump from single to double layer occurs.

have dimensions of energy. Due to our suppression of the thermal energy scale in this derivation, the corresponding energy denominator is missing here. We come back to this point in the next section.

Taken together the first two terms on the right hand side of Eq. 7 account for spin diffusion induced by that nearest neighbor coupling and the local exponential relaxation to zero of the average $s_i$ of the microscopic layer variable $\sigma_i$. Of course, the final term on the right hand side shifts the time-stationary value of $s_i = S$ to

$$S = -e^{2J} \tanh{[h_{\text{eff}}]}. \tag{9}$$

This result is the usual mean-field solution of the Ising model, at least in the limit of small $h$, where the Glauber dynamics assumption is applicable.

If one were to assume that the spin dynamics were fast, $\tau_s \ll \dot{h}_{\text{eff}}/h_{\text{eff}}$, the mean spin variables would simply track the effective magnetization. The spin dynamics representing the formation of the double layer would be slaved to the state of raft compression and independent of compression rate. The other limit, in which we assume that the spin variables are slow compared to the rate at which the elastic variables relax, however, frees the double layer formation to follow its own dynamics in a manner that depends on the compression rate of the raft. This latter case is also reasonable since the formation of the double layer is slow, relying on rare stochastic events. The elastic relaxation of the bubble raft, on the other hand, is rapid. It occurs on time scales associated with the diffusive relaxation of compression in the elastic network of bubbles coupled to the viscous subphase. Consequently, we explore the nonequilibrium dynamics

of the coupled elastic and spin system, where the transitions between spin up and spin down are slow in order to address the formation of particular transient structures obtained in the experiments as a function of *compression rate*.

To explore the dynamics of the coupled system of spins and elastic displacement variables, we numerically solve Eqs. 4 and 5, but replacing the stochastic spin variables $\sigma_i$ by their ensemble average $s_i$ to close the set of dynamical equations. These equations are solved subject to boundary conditions such that the bubble layer is contained to move with a given velocity at the boundaries

$$u_1(t) = -u_N(t) = vt, \tag{10}$$

and that the system starts with a double layer at the boundary

$$s_1 = s_N = +1, \tag{11}$$

due to the favorable bubble-wall interaction. To compare our results to experiment, we note that the probability of observing a double layer at $i$ is related to the mean-field spin variable by $P_i = (s_i + 1)/2$. Thus, our solutions for $s_i$ may be directly compared to the measured probability distributions as a function of both compression speed $v$ – see Eq. 10 – and the state of compression $c = \Delta L/L$. A representative sample of such solutions are shown in Fig. 4.

Figure 4 shows the $s_i$ for various values of compression speed, increasing down the column. It is clear that the main qualitative features of the experiment are reproduced here. First, at sufficiently slow compression speeds, the double layer regime begins at the walls (where double layers are heterogeneously nucleated) and a single front of single- to double-layer transition moves inward with compression until the entire raft becomes a double layer. At very high compression speeds, one observes a spatially uniform increase in the transition probability from single to double layer, as experimentally observed – see Fig. 3. The most interesting result of the theoretical analysis occurs at intermediate compression speeds where multiple steps in the probability distribution for double layers appear. One observes at least two such steps in the numerical results presented in the middle panel of Fig. 4. There is some evidence of such step-like features in the experimentally observed distribution of single and double layers – see Fig. 3b. The theory also predicts the formation of a hierarchy of many nested steps appearing in the double-layer probability in sheets with much higher compressional moduli as compared to the bubble raft. An example of this theoretical result is shown in Fig. 5, where one observes six such nested steps.

## C. Time scales and comparison to experiment

In order to make a comparison between theory and experiment, a discussion of time and length scales is in

order. It is most simple to introduce nondimensional time and space variables: $\bar{t} = t/\tau_s$ and $\bar{u} = u/a$ respectively. In terms of these variables, the relaxation of compression is now given by

$$D = k\Gamma\tau_s, \qquad (12)$$

and the dimensionless $\Delta$ appearing in Eq. 5 is replaced by $\bar{\Delta} = \Delta/a = 1/2$. In the spin dynamics, given by Eq. 7, the spin relaxation time scale is now unity. The effective "magnetic field" $h_{\text{eff}}(\bar{t})$ now depends on the dimensionless time $\bar{t}$ via

$$h_{\text{eff}}(\bar{t}) = \tanh\left\{ h + k\bar{\Delta}a^2 \left[ \bar{u}_{i+1}(\bar{t}) - \bar{u}_i(\bar{t}) \right] \right\}. \qquad (13)$$

Finally, in these nondimensionalized units, the compression speed is given by

$$\bar{V} = v\tau_s/a. \qquad (14)$$

The dimensionless speeds corresponding to the experimental fast and slow compressions are then $1.72 \times 10^{-1}$ and $1.72 \times 10^2$ respectively.

The parameter $D$ physically represents the separation of time scales between the equilibration of in-plane stresses occurring on the time scale of $1/(k\Gamma)$ – see Eq. 5 – and the transition time for single to double-layer exchange, given by $\tau_s$. For our model to be relevant, we need the former to be much faster than the latter, or a large value of $D$. The value of $D$ in the experiment can be estimated from the lifetime of the double layers and the relaxation of compression waves across the system. Given the observed lifetime of small double layer regions, we take $\tau_s \sim 10s$. From the observed rapid (on the order of milliseconds) relaxation of compression across the raft as a whole, we estimate $D \sim 10^4$.

We now turn to the estimate of the other parameters entering the model. We may express the bubble spring constant in terms of the bubble surface tension $\mathcal{T}_{\text{surf}}$ and radius $a$, using $k \sim \mathcal{T}_{\text{surf}}/a \approx 10$ dyn/mm$^2$. Thus, we find that $k\bar{\Delta}a^2 \sim 2.5$erg. If we associate the magnitude of the symmetry breaking field $h$ with the work done against buoyancy $\sim \rho g(4\pi/3)a^3 \times a$ in pushing a bubble down to the second layer in water of density $\rho \sim 1$g/cc$^3$, we find that $h \sim 0.4$ erg. Although this result justifies our assumption that $h \ll k\bar{\Delta}a^2$, we still do not know the magnitude of the noise temperature in the system. Consequently, we treat the overall scale of $h, J$ as adjustable parameters, consistent with the fact that $h \ll J \sim k\bar{\Delta}a^2$.

## V. DISCUSSION

Using these numerical estimates, we find that the experimental data in the fast and slow compression regimes is consistent with the model prediction of an inwardly propagating wave of double-layer formation in the slow compression regime and a spatially homogeneous flip in to the double layer at high compression velocities. In all cases, the system accommodates the loss of surface area first by uniform compressive strain in the single-layer raft (since $D \gg 1$, elastic strain relaxes across the system rapidly), but eventually this compressive strain is relaxed by local transitions from single to double layers. At slow compression rates, this transition begins at the walls, due to heterogeneous double-layer nucleation there, and propagates inward with two symmetrically placed transition fronts, in order to minimize the domain-wall energy associated with $J$. At sufficiently high compression rates, the elastic system is driven to higher compressive strains as the single- to double-layer transition becomes trapped in a metastable state. Eventually, the energetically-unfavorable, high-compression single layer jumps homogeneously into the favored double-layer state.

Most interestingly, the model makes the nontrivial prediction of a stepwise double-layer probability distribution at intermediate compression rates. The dynamical crossover from the slow dynamics of a single propagating front to the fast dynamics of homogeneous transition proceeds via the formation of multiple propagating fronts of single- to double-layer transition probability. In fact, for sufficiently large $J$ and for sufficiently high $k$, one can follow the transition from a single front to homogenous single- to double-layer transition through a continuous *reduction* of the number of steps. One may consider the single front to be in actuality the maximal number of steps; the step size has been reduced to the microscopic length cutoff (here the bubble size) causing these steps to merge into a single smooth front. As the compression velocity increases, the number of steps decreases and consequently the typical step length grows. Eventually this step length approaches the system size. At this point the transition from single to double layer is effectively homogeneous in space, and we recover the observed fast compression dynamics.

As an example of transition region, one may observe in Fig. 5 six distinct steps in the transition regime between the (slow compression) front and the (fast compression) homogeneous jump. It is to be noted that in order to resolve this larger number of steps, the spring constant had been increased to $10^4$. As the spring constant is reduced (and as $J$ is reduced) the steps become less sharp so that the full hierarchy of steps cannot be resolved in the dynamics. Using the parameters consistent with the current set of bubble raft experiments, we expect to resolve no more than one or two steps.

The experimentally observed difference between single- to double-layer dynamics associated with respectively slow and fast compression is clearly reproduced by the model. In addition, the experimental results, while noisy, support the basic step-forming picture that emerges from the model in that we see secondary fronts at intermediate compression rates. The formation of these nested fronts is a nontrivial prediction of the model, and their experimental observation validates the basic structure of the analysis. We cannot yet experimentally observe the much richer structure of a large number of steps. Based on our

numerical solutions of the model, however, we conclude that the bubble raft is insufficiently stiff elastically (too small $k$) to support the full step hierarchy. With our current bubble radius of a few tenths of a mm, the elastic constant is on the order of 10 dyn/mm$^2$. Varying the bubble diameter by 2 - 3 orders of magnitude in future experiments will allow us to explore a similar range of elastic constants.

Even if the stiffness of the raft were increased, observing the birth of multiple fronts in experiment (e.g., as in the theoretical prediction shown in Fig. 5) would still prove difficult. This difficulty stems from the fact that, as the number of fronts grows, the compression-rate range consistent with their formation becomes quite narrow. Nevertheless, we believe that finding experimental support (or refutation) of this model has broad implication for the nonlinear elasticity of a variety of biological and synthetic materials, as outlined in the introduction. Moreover, this work suggests a number of intriguing extensions, such as the correlation between the collapse and the applied force under compression, understanding the mechanics of these systems under more complex induced strains (as opposed to uniform compression), and experiments in which one directly drives the internal variable to induce new stresses into the elastic manifold via local and incompatible changes to the stress-free, reference state. Such experiments will have important implications for the charging of super-capacitors. Finally, we note that same analysis provided here for amorphous, high symmetry elastic systems, can be extended to lower symmetry crystalline materials. These allow more complex changes to the local reference state beyond simple changes in area. In addition, they allow the interaction of changes in the reference state and local topological defects in the structure. These extensions can also be pursued using bubble rafts as a model system providing a (perhaps unique) combination of access to collective mechanics and the tracking of the microscopic strain and internal state variables in nonequilibrium systems.

[1] Jean-Baptiste Salmon, Annie Colin, Sébastien Manneville, and François Molino, Phys. Rev. Lett. **90**, 228303 (2003).
[2] Peter D. Olmsted, Rheol. Acta **47**, 283-300 (2008).
[3] Bo Li, Yan-Ping Cao, Xi-Cao Feng, and Haujian Gao, Soft Matter **8**, 5728-5745 (2012).
[4] Simona Cocco and Rèmi Monasson, Phys. Rev. Lett. **83**, 5178 (1999).
[5] Paul A. Wiggens, et al., Nat. Nanotech. **1**, 137 (2006).
[6] Chiao-Yu Tseng, Andrew Wang, Giovanni Zocchi, Biljana Rolih, and Alex J. Levine, Phys. Rev E **80**, 061912 (2009).
[7] Hao Qu, Chiao-Yu Tseng, Yong Wang, Alex J. Levine, and Giovanni Zocchi, Europhys. Lett. **90**, 18003 (2010).
[8] Arthur A. Evans and Alex J. Levine, Phys. Rev E **85**, 051915 (2012).
[9] Buddhapriya Chakrabarti and Alex J. Levine, Phys. Rev E **71**, 031905 (2005).
[10] Buddhapriya Chakrabarti and Alex J. Levine, Phys. Rev E **74**, 031903 (2006).
[11] Boris I. Shraiman, Proc. Natl. Acad. USA **102**, 3318 (2005).
[12] Fabien Montel, et al., New J. Phys. **14**, 055008 (2012).
[13] Celeste M. Nelson, et al., Proc. Natl. Acad. USA **102**, 11594 (2005).
[14] Haiyi Liang and L. Mahadevan, Proc. Natl. Acad. USA **108**, 5516 (2011).
[15] Janet M. Tse, et al., Proc. Natl. Acad. USA **109**, 911 (2012).
[16] T. Brezesinski, et al., ACS Nano **4**, 967 (2010).
[17] Lawrence Bragg and W.M. Lomer, Proc. Royal Soc. Lond. A **196**, 171 (1949).
[18] Mark J. Bowick, Luca Giomi, Homin Shin, and Creighton K. Thomas, Phys. Rev E **77**, 021602 (2008).
[19] John Lauridsen, Michael Twardos, and Michael Dennin, Phys. Rev. Lett. **89**, 098303 (2002).
[20] Michael Twardos and Michael Dennin, Phys. Rev. E **71**, 061401 (2005).
[21] Kapilanjan Krishan and Michael Dennin, Phys. Rev. E **78**, 051504 (2008).
[22] Denis Weaire, Joseph D. Barry, and Stefan Hutzler, J. Phys. Cond. Mat. **22**, 193101 (2010).
[23] Peter Schall and Martin van Hecke, Ann. Rev. Fluid Mech. **42**, 67 (2010).
[24] Roy J. Glauber, J. Math. Phys. **4**, 294 (1963).
[25] See, for example Z.R. Yang, Phys. Rev. B **46**, 11578 (1992).
[26] P.C. Hohenberg and B. I. Halperin, Rev. Mod. Phys. **49**, 435 (1977).
[27] Howard A. Stone and Armand Ajdari, J. Fluid Mech. **369**, 151 (1998).
[28] C.-C. Kuo and Michael Dennin, J. Rheol. **56**, 527 (2012).
[29] M. Dennin, Phys. Rev. E 70, 041406 (2004)
[30] We justify the reduction of the two dimensional system to a one dimensional analysis as follows. In the images of the compressed layers, one observes patterns of single and double layers consistent with a uniform probability distribution in the direction ($y$) transverse to the compression. Based on this observation and to improve the reproducibility of the data, experimental collapse data were averaged in thin strips whose long axis lies in the transverse direction. Thus, we have access to only $\mathcal{P}(x,t)$, which is given by the spatial average of $P$ over the $y$-direction, and we believe that the full probability distribution depends at most weakly on the transverse direction.